Engineering catalyst supports to stabilize Pd/PdO 2D rafts for water-tolerant methane oxidation

Haifeng Xiong
Xiamen University https://orcid.org/0000-0002-3964-4677
Deepak Kunwar
University of New Mexico
Carlos García-Vargas
Washington State University https://orcid.org/0000-0001-7486-9604
Griffin Canning
University of New Mexico
Dong Jiang
Washington State University
Xavier Isidro Pereira Hernandez
Washington State University https://orcid.org/0000-0002-7020-0011
Sen Lin
Fuzhou University https://orcid.org/0000-0002-2288-5415
Qiang Wan
Fuzhou University
Stephen Purdy
Purdue University
Jeffery Miller
Purdue University
Kevin Leung
Sandia National Laboratories
Stanley Chou
Sandia National Lab
Hidde Brongersma
ION-TOF GmbH
Rik Veen
Tascon GmbH
H. Guo
University of New Mexico https://orcid.org/0000-0001-9901-053X
Yong Wang
Washington State University
Abhaya Datye (datye@unm.edu)

University of New Mexico https://orcid.org/0000-0002-7126-8659

Article

Keywords: Atom trapping, 2-D-raft, Single atom catalysis, Nucleation sites

Posted Date: December 14th, 2020

DOI: https://doi.org/10.21203/rs.3.rs-113744/v1

Version of Record: A version of this preprint was published at Nature Catalysis on October 18th, 2021.
See the published version at https://doi.org/10.1038/s41929-021-00680-4.

Abstract

The size and morphology of the active phase (metal or metal oxide) are critical for the performance of heterogeneous catalysts. Conventional approaches for catalyst synthesis involve the modification of pore size and structure, the use of ligands to anchor the metal during preparation or the use of nanostructured oxides with well-defined facets to provide suitable sites for metal nucleation and growth. However, these approaches may not yield durable catalysts for high temperature applications, such as the treatment of unburnt methane from natural gas fueled engines. Here we demonstrate an approach that relies on the trapping of metal single atoms on the support surface, in thermally stable form, to modify the nature of deposited metal/metal oxide clusters. By anchoring Pt ions on the catalyst support we can tailor the morphology of the deposited phase. In particular, two-dimensional (2-D) rafts of Pt/PtO_x on the engineered catalyst support are formed by this approach, as opposed to three-dimensional (3-D) metal oxide nanoparticles on conventional supports. Adopting this approach for the synthesis of bimetallic catalysts via addition of Pd to the atom-trapped catalyst support ($Pt@CeO_2$) we found that the resulting $Pd/Pt@CeO_2$ catalyst provides improved thermal stability and water tolerance during methane oxidation. We attribute the improved performance to the 2-D morphology of the Pd/PdO phase present on the atom-trapped catalyst support. The results show that modifying the support by trapping single atoms could provide an important addition to the toolkit of catalyst designers to engineer catalyst supports for controlling the nucleation and growth of metal and metal oxide clusters in heterogeneous catalysts.

1. Introduction

The control over the size, morphology and oxidation state of clusters and nanoparticles is important for achieving optimum performance in heterogeneous catalysis. There are limited means available for catalyst designers to influence the nature of the active phase, especially when the catalysts are subjected to elevated temperatures. The most widely used approach for industrial catalysts involves adsorption of the metal salt precursor on an oxide support[1], via the methods of deposition-precipitation or strong electrostatic adsorption (SEA)[2]. Using these approaches, it is possible to achieve atomic dispersion of the deposited metal on a number of catalyst supports[3-6]. The interaction between the metal salt precursor and the functional groups on the surface (hydroxyls) determines the surface concentration of the dispersed phase. The nature and morphology of the dispersed phase depends on the surface structure of the oxide support[7, 8], which can be manipulated by using faceted oxides as supports, or by introducing ligands on the support[9]. By pre-calcining the support, the number of hydroxyls on the support can be changed, which allows some control over the metal deposition (Scheme 1a).

However, once the catalyst is treated at high temperatures, the mobility of the deposited metal leads to formation of thermodynamically stable structures, where the influence of the initial preparation steps is lost. Here we explore an alternate approach where we trap metal atoms on the support to modify the

nucleation and morphology of the dispersed phase (Scheme 1b). Since the trapped metal atoms are stable at high temperatures, we can generate a catalyst suitable for high temperature applications such as methane oxidation.

Methane combustion catalysis is becoming increasingly important to address the emission of unburned methane associated with the widespread use of natural gas as a clean fuel for vehicles and for power generation. Pd-based catalysts show the highest activity for methane oxidation, however they suffer from rapid deactivation due to the presence of H_2O and sintering of the Pd phase[10]. Because of the excess O_2 present in the reactant stream, the stable phase of Pd under reaction is PdO. The sintering of Pd catalysts under steam is ascribed to the formation and migration of mobile Pd-OH entities in the presence of H_2O molecules[11], which are strongly adsorbed on the PdO surface. The binding of H_2O to the PdO also causes poisoning of the surface sites for methane oxidation[12]. Such surface poisoning by steam is confirmed by the fact that the surface coverage of CH_4 in the presence of water vapor is limited to only 3% of the saturation coverage of a pure CH_4 layer on PdO (101)[13]. In our previous work, when Pd catalysts were reduced prior to reaction, we observed enhanced low-temperature reactivity[14]. Similar enhanced reactivity due to pre-reduction of Pd catalysts (also termed in-situ activation) has been reported by other workers[15, 16]. We attribute this higher reactivity to a different form of surface Pd oxide formed on the surface of the reduced Pd catalyst (in contrast to bulk PdO). This is consistent with DFT calculations which show that a surface oxide is more active than bulk PdO nanoparticles[17, 18]. However, when Pd based catalysts are used for methane combustion, the metal Pd nanoparticle transforms to PdO, leading to the decrease in catalytic activity[19]. A well-known approach for improving the stability and reactivity of Pd based catalysts is to add Pt, which stabilizes the Pd phase in a metallic state by forming bimetallic PtPd even under oxidizing conditions[20], leading to enhanced resistance to adsorption of water molecules. However, the bimetallic PtPd catalysts are not as resistant to sintering as PdO catalysts, showing the formation of large alloy PtPd particles (> 20 nm) and declined catalytic reactivity[14, 21]. Therefore, there is an urgent need to develop methods to form an active Pd phase which is resistant to H_2O poisoning and to catalyst sintering[22].

In this work, we have modified the catalyst support via strongly bound Pt single atoms (atom trapping[23-25] - high temperature vapor phase synthesis), to control the nature of the metal and metal oxide phase. We show that a 2D morphology of the Pd/PdO phase synthesized with this approach is thermally-stable and resistant to water poisoning. The catalysts thus prepared overcome the disadvantages of large PdO particles which are readily poisoned by water, leading to decreased activity, or single atom Pd on the support which is less active for methane oxidation[26].

2. Methods

2.1. Catalyst preparation

The initial experiments to investigate the role of atom trapped Pt were performed with the commercial ceria (Solvay-Rhodia HS 5) henceforth referred to as HSA ceria since it has a higher surface area than the ceria prepared by calcination of $Ce(NO_3)_2$ which was used for the Pd-Pt catalysts. To prepare engineered CeO_2, tetraamine platinum nitrate solution was impregnated onto CeO_2 powder by conventional wet impregnation, followed by drying at 120 ^oC for 12 h. The powder was then calcined at 800 ^oC for 10 h in flowing air. The obtained materials were denoted as 1Pt@CeO_2 and 3Pt@CeO_2, corresponding to the Pt loadings of 1 and 3 wt.%, respectively. The high temperature treatment causes a drop in BET surface area, from 135 m^2/g for the as-received ceria to 60 m^2/g for the pure ceria (referred to henceforth as PS or pre-sintered ceria), 78 m^2/g for 1Pt@CeO_2 and 100 m^2/g for the 3Pt@CeO_2 sample. The Pt interacts strongly with the ceria surface, pinning defect sites and slowing the rate of ceria sintering[24, 27].

The nucleation and growth of Pt on PS CeO_2 support (pre-calcined at 800 °C in air for 10 h) and the 1Pt@CeO_2 (subjected to a similar thermal treatment) helped identify the role of trapped Pt atoms during catalyst preparation. An appropriate amount of tetraamine platinum nitrate ($Pt(NH_3)_4(NO_3)_2$) was added to each support followed by drying at 120 ^oC for 12 h and calcination at 500 ^oC for 4 h in air. The total Pt loading for each catalyst was 3 wt.% Pt and the samples were denoted as 2Pt/1Pt@CeO_2 and 3wt%Pt/PS-ceria.

For the methane oxidation study, we used ceria powder prepared in the laboratory via decomposition of $Ce(NO_3)_2$, as described in our previous work[23]. This ceria powder has a BET surface area of 85 m^2/g as-prepared. To prepare the engineered catalyst support, we used 2 wt% Pt via impregnation, drying in air, calcination at 500 ^oC following by aging in air at 800 ^oC for 10 h. This catalyst support is denoted as 2Pt@CeO_2. Palladium nitrate (1.09 wt% Pd) was deposited on the 2Pt@CeO_2 by wet impregnation, followed by drying at 120 ^oC for 12 h and calcining at 500 ^oC for 4 h in air. The catalyst was denoted as 1Pd/2Pt@CeO_2. To provide a comparison, we also prepared two reference samples of 1Pd/CeO_2 (1.09 wt%Pd) and (1Pd+2Pt)/CeO_2 containing the same loading of metal as the 1Pd/2Pt@CeO_2. For the reference (1Pd+2Pt)/CeO_2 catalyst (BET surface area: 67 m^2/g), the palladium (II) nitrate solution was impregnated onto the CeO_2 first, then dried at 120 ^oC in air for 12 h. After calcination at 500 ^oC in air for 4 h, tetraamineplatinum nitrate (2 wt.% Pt) was impregnated onto the material progressively, followed by drying at 120 ^oC for 12 h in air and calcining at 500 ^oC for 4 h in air. The reference 1Pd/CeO_2 (1.09 wt%Pd) sample was prepared by impregnating appropriate amount of palladium (II) nitrate solution onto the CeO_2. Then, the sample was obtained after drying at 120 ^oC in air for 12 h and calcining at 500 ^oC in air for 4 h.

2.2. Catalyst characterization

Aberration corrected scanning transmission electron microscopy (AC-STEM) was carried out using a FEI Titan Themis transmission electron microscope equipped with the Gatan K2-IS camera. We also used a JEOL ARM200CF microscope for some of the samples. In each case, the sample powders were deposited on holey carbon films after being dispersed in ethanol. The single Pt atoms on CeO_2 can be clearly seen in the AC-STEM dark field images. Low energy ion scattering (LEIS) was used to quantify the concentration of Pt atoms on the catalyst surface. This technique selectively detects the topmost atoms and was carried out using an IONTOF Qtac100 instrument[28]. The dedicated LEIS instrument was equipped with a double toroidal analyzer for the energy analysis of the backscattered ions and the analyzer has a large solid angle of acceptance (full 360° azimuth), while the scattering angle is fixed at 145°. In combination with parallel energy detection, this gives a high sensitivity while maintaining the mass resolution. He^+ and Ne^+ with ion energy 3 and 5 keV and current 5 and 2 nA, respectively, were used to analyze the surface concentration of Pt^{2+} ions in the catalysts. The area scanned per sample by these two ions was 2 × 2 mm^2 and the ion flux used was 1.4 × 10^{14} ions/cm^2 and 2.8 × 10^{13} ions/cm^2 respectively. The spectra for the Pt reference were analyzed within a 1.5 × 1.5 mm^2 sputter crater over an area of 1 × 1 mm^2. The analysis time was adjusted such that the surface damage was the same as for the other spectra. Assuming a sputter coefficient of 0.1 for He and 1 for Ne, this will lead to a surface damage of 1% and 2% at the end of the analysis. X-ray photoelectron spectroscopy (XPS) was performed using a Kratos Axis Ultra photoelectron spectrometer equipped with a monochromatic Al Kα source operating at 300 W. The base pressure was 2.7 × 10^{-8} Pa and operating pressure was 2.7 × 10^{-7} Pa. Analysis of the XPS spectra was performed using CASA XPS software. X-ray absorption spectroscopy was performed at the materials research collaborative access team (MRCAT) bending magnet and insertion device lines at the Advanced Photon Source, Argonne National Laboratory. Measurements at the Pd K edge were performed in transmission mode using a set of 3 ion chambers which allowed for concurrent measurement of a Pd foil energy reference. Measurements at the Pt L3 edge were performed in fluorescence mode using a Lytle detector with a zinc foil filter used to reduce background fluorescence. At both edges, sample wafers were pressed in a stainless steel sample holder and measured at room temperature in air. Data analysis was performed using Artemis and Athena in the Demeter software suite[29] with phase and amplitude functions generated by FEFF using bulk references. At each edge, the amplitude reduction factor (S_0^2) was determined by fitting the first shell scattering of the respective metal foil. The obtained S_0^2 was then fixed in catalyst samples. A spherical nanoparticle shape function was used in the modeling of Pd/Pt@CeO_2 at the Pd K edge[30]. Full model and fit details are given in the supplemental information.

2.3. Catalytic reactivity measurements

CO oxidation was chosen as a probe reaction. The reaction rate measurements were performed using 1/4 in. diameter U-tube with 20 mg of sample. The gas flow rates for CO oxidation were the following: CO 1.5 mL/min, O_2 1 mL/min, and He 75 mL/min and temperature ramp rate was at 2 °C/min. The as-prepared,

air-exposed catalyst was loaded into the reactor and temperature was increased to 300 °C under He. Once at 300 °C, a pretreatment with 10% O_2 was performed for 30 min. The gas was then switched to He and the catalyst was cooled to the reaction temperature. Subsequently, CO oxidation kinetic measurements were performed. The total pressure during CO oxidation was 83.3 kPa, the atmospheric pressure in Albuquerque. The products were analyzed by an Agilent Micro GC 490.

Catalytic methane (CH_4) combustion was performed using a fixed bed flow reactor. 60 mg of catalyst powder was diluted by 600 mg SiC to guarantee isothermal conditions. The catalyst bed was packed between two quartz wool plugs inside a ½ inch (I.D.) quartz tube. The reaction was performed at atmospheric pressure. The reaction gas consisted of 680 ppm CH_4, 14 vol % O_2 and 5 vol % CO_2 balanced with N_2 with a total flow of 300 mL/min. Different concentrations of steam (H_2O) were introduced by flowing the reaction gas through a temperature-controlled bubbler. The effluent gas was analyzed by an online MKS equipped with a detector. For light-off measurements, the samples were heated from room temperature to 650 ^oC with a ramp of 5 ^oC/min in reaction gas. After each light-off test, the system was cooled down in a O_2/N_2 atmosphere. Stability under different dry/wet conditions was also evaluated by time-on-stream measurements.

2.4. Density functional theory calculations

All spin-polarized Density Functional Theory (DFT) calculations were performed using the Vienna *Ab initio* Simulation Package (VASP)[31, 32]. The valence electrons were represented by plane waves with a cutoff energy of 400 eV, augmented with the projector-augmented wave (PAW) pseudopotentials for the core electrons[33]. A Hubbard-like term was added in the so-called DFT+*U* treatment with U = 4.5 eV applied to the Ce 4f states[34]. For bulk surfaces, the atoms in the top five layers of PdO(101) and the top two layers of Pd(111) were fully relaxed. The reciprocal space was sampled with a *k*-point mesh of 3 × 3 × 1. For the Pd raft on the engineered Pt@CeO_2 support via atom trapping, we modeled the slab with 1 Pd(111) layer and 6 CeO_2(111) layers, the slab was generated by a $2\sqrt{2}\times2\sqrt{2}$ unit CeO_2(111) covered by a $\sqrt{13}\times\sqrt{13}$ layer of Pd(111), and optimized distance between the Pd(111) layer and CeO_2(111) was 2.13 Å. The reciprocal space was sampled with a *k*-point mesh of 1 × 1 × 1. During geometry optimization, the atoms in the bottom three atomic layers were fixed while others were fully relaxed. In these cases, the exchange-correlation potential was treated by the PW91 exchange-correlation functional[35]. A vacuum space larger than 15 Å was set between periodic slabs in order to avoid the artificial interactions along the z-direction. Electronic energy was converged below a threshold of 10^{-4} eV, while the force acting on each atom was less than 0.05 eV/Å. Climbing image nudged elastic band (CI-NEB) approach was used to determine the reaction pathway[36, 37].

3. Results And Discussion

3.1. Engineering of the catalyst support via atom trapping

In this work, we first modified the ceria with atomically dispersed Pt to prepare the catalyst support (Fig. 1a). This involves deposition of a Pt precursor (1 wt% Pt) on the ceria support, then heating to 800 ^{o}C in air for 10 h. Since the Pt is present in atomically dispersed form, we will refer to this support as 1Pt@CeO_2 (Fig. 1b). Next we deposited additional 2 wt% Pt on this engineered ceria support. We found that the added Pt does not form atomically dispersed species as is typically seen on ceria supports[28, 38] (see Fig. 1c-d and Supplementary Figure 1). It appears that the initial high temperature treatment has eliminated the sites on which atomically dispersed Pt would reside. Instead we see the formation of 2-D rafts as shown in Fig. 1c-d and Supplementary Figure 1 (labelled by both boxes and arrows), as revealed by the uniform contrast of the domains from center to edge. The edge-on views confirm the 2-D nature of the deposited Pt and the top-down views show the size of the Pt domains to be ~1 nm. EXAFS measurements of this catalyst (Supplementary Figure 2 and Supplementary Table 1) confirm that this catalyst contains oxidized Pt but has no Pt-Pt neighbors, i.e. no Pt metal clusters. This catalyst (which is termed as 2Pt/1Pt@CeO_2) contains Pt rafts instead of 3-D metal or oxide clusters.

The CO oxidation reactivity for this 2Pt/1Pt@CeO_2 catalyst (containing a total of 3 wt% Pt) is greater than a 3Pt@CeO_2 prepared via atom trapping (Fig. 2). This is in agreement with a recent work showing that clusters of Pt oxide (for example Pt_8O_{14} containing Pt-O-Pt sites) are more active in CO oxidation[39] than single atom Pt. We should note that even higher CO oxidation reactivity can be achieved by reducing Pt/CeO_2 catalysts[38, 40], but our focus here is on the oxidized state of the catalyst which is encountered during lean methane oxidation. Under the lean conditions (excess oxygen), the CO oxidation reactivity is reproducible over multiple runs. Low Energy Ion Scattering (LEIS, Fig. 2a and Supplementary Table 2), which is exquisitely surface sensitive, shows that the measured Pt concentration on the 2Pt/1Pt@CeO_2 catalyst (1.8 atoms/nm^2) exceeds the expected surface concentration (~ 1.2 atom/nm^2) calculated based on the Pt content and the BET surface area (Supplementary Table 2). In our previous work on atom-trapped Pt/CeO_2 we reported the upper limit of Pt surface concentration in single atom catalysts on this same ceria support was ~1 atom/nm^2.[28] These results should be put in context with the surface concentration of Ce on the CeO_2 (111) facet which is 7.9 atoms/nm^2 [41] and the Pt surface concentration in an oxidized Pt foil which is 9.0 atoms/nm^2 (Supplementary Table 2). Therefore, the observed surface concentration for 2-D Pt rafts of 1.8 atoms/nm^2 significantly exceeds that expected from atomically dispersed Pt and is consistent with the presence of Pt rafts on ceria (111) surface facets, with a preferred orientation due to prominent (111) facets leading to more prominent exposure of Pt as seen via AC-STEM (Fig. 1c and d).

These results show that by starting with a catalyst support containing 1 wt% of strongly bound Pt single atoms, we cause the added 2 wt% Pt to form 2-D rafts. To investigate whether this 2-D raft morphology was simply a result of the high temperature treatment of the ceria, we prepared a catalyst support by heating the ceria support to 800 ^{o}C (which we term pre-sintered or PS ceria). As shown in Supplementary

Figure 3, heating ceria (800 ^{o}C, 10 h) causes a modest loss in surface area of the support (Supplementary Figure 3d) also leading to well defined ceria (111) surface facets. When we deposited 3 wt% Pt on the PS-ceria and calcined the sample at 500 °C, we observed randomly oriented Pt in the form of 3-D nanoparticles (Supplementary Figure 3c). Therefore, the formation of 2-D rafts on 2Pt/1Pt@CeO_2 is very unusual and not simply a result of the high temperature treatment of the ceria support. Using the 1Pt@CeO_2 as a support modifies the nucleation of the deposited Pt forming 2-D rafts instead of 3-D nanoparticles which are seen on PS-ceria. The facile formation of Pt 2-D rafts and the superior reactivity of this catalyst compared to single atom Pt is consistent with the results from our DFT calculations (Supplementary Figures 4 and 5). In summary, our results show that when the CeO_2 support is modified through the method of atom trapping, the strongly bound Pt single atoms act as templates, helping the Pt that is deposited on this support to form 2-D rafts, presenting superior CO reactivity compared to the Pt single atom catalyst on CeO_2.

3.2. Methane oxidation on Pd deposited on the engineered catalyst support

Inspired by the above observations and results, we deposited Pd (1.09 wt%) on the engineered ceria support prepared by atom trapping of Pt as described in the previous section. To achieve a 1:1 Pd:Pt molar ratio, we used a catalyst support containing a Pt loading of 2 wt.% prepared via atom trapping (800 °C in air for 10 h) using ceria prepared by decomposition of $Ce(NO_3)_2$, which we refer to as polyhedral ceria (PHC). The performance of this catalyst (1Pd/2Pt@CeO_2, Pd:Pt atomic ratio=1:1) was compared with other catalysts on the same ceria support, including the 2Pt@CeO_2 used to prepare 1Pd/2Pt@CeO_2 and 1Pd/CeO_2 prepared by impregnation. The reactivity was measured in a fixed bed reactor using a gas mixture that resembles the effluent encountered during methane oxidation from vehicular exhaust (680 ppm CH_4, 14 vol % O_2, 5 vol % CO_2 balanced with N_2 with a total flow of 300 mL/min). For some of the experiments, we added water vapor to investigate the water tolerance of these catalysts. The light-off curves show that the 1Pd/2Pt@CeO_2 catalyst is more active than the oxidized 2Pt@CeO_2 and 1Pd/CeO_2 catalysts containing the same amount of the corresponding metal atoms under dry methane oxidation conditions (Fig. 3a). The 1Pd/2Pt@CeO_2 catalyst also shows improved low temperature reactivity compared to the reference (2Pt+Pd)/CeO_2 catalyst prepared using the same ceria support (2 times higher at 350 ^{o}C). The reference catalyst involved a conventional preparation via impregnation and calcination at 500 °C in air, but without any high temperature (800 °C) treatment.

To test the catalyst stability with & without added steam, methane oxidation was carried out at 500 ^{o}C and the conversion was kept between 90-100% by varying the space velocity (Fig. 3b and c). The 1Pd/2Pt@CeO_2 catalyst did not suffer a significant loss of reactivity when switching from dry to steam-containing methane feeds (4% loss in 5 v/v% water and 15% loss in 10 v/v% water, Fig. 3b) and the reactivity recovered after stopping water vapor flow. This shows an improvement in water tolerance for the Pd/2Pt@CeO_2 catalyst. Multiple runs of this catalyst also demonstrate the reproducibility of the data

(Supplementary Figure 6a). The light off curves in the presence of varying amounts of steam (4% and 10%) are shown in the supporting information (Supplementary Figure 6b).

While methane oxidation catalysts operate under lean conditions (excess oxygen), we have seen in previous work that reduction of the catalyst forming metallic particles, or periodic pulses under reducing conditions, lead to enhanced reactivity[14-16]. In previous work, we have found that CO reduction at 275 °C is sufficient to reduce single atom catalysts and achieve optimal CO oxidation reactivity[38]. Therefore, we tested the performance of these catalysts after CO reduction (Fig. 3c). We see definite improvement in the light off curve for the bimetallic as well as the monometallic reduced 2Pt@CeO_2 and 1Pd/CeO_2 catalysts (Fig. 3c), but the bimetallic Pd/2Pt@CeO_2 catalyst performs better than monometallic Pt or Pd and is stable at high reaction temperatures (> 550 ^oC). At these high conversions, the methane is consumed so the catalyst is being subjected to an oxidizing atmosphere, which shows the improved thermal stability of this catalyst. While the Pd-only catalyst shows similar stable performance under oxidizing conditions (since it forms PdO, which is known to be active at high temperatures), the Pt only catalyst suffers a loss in reactivity. We attribute this loss of activity to the oxidation of the Pt nanoclusters and also possible re-dispersion to form Pt single atoms under oxidizing conditions at elevated temperature (Fig. 3c).

While the reduced Pd and Pt catalysts show improved reactivity after reduction (Fig. 3c), the performance of these catalysts cannot be sustained during methane oxidation and in the presence of water vapor (Fig. 3d). These catalysts suffer a major loss in reactivity due to oxidation of the metal and poisoning by water vapor. In contrast, the Pd/2Pt@CeO_2 catalysts shows only a slight drop in for the long term run at 500 ^oC (Fig. 3d). This drop is likely caused by the large amount of water molecules produced in the reaction at the high conversion of this test[42]. These results show that under the conditions of lean methane oxidation, the contribution from the starting single atom 2Pt@CeO_2 is negligible. Since the bimetallic catalyst Pd/2Pt@CeO_2 and the Pd/CeO_2 contain similar amounts of Pd, the enhanced performance of the former catalyst must be attributed to the morphology of the Pd/PdO phase present on the 2Pt@CeO_2 support, which is what we describe next.

To morphology of the Pd/2Pt@CeO_2 catalyst was studied via AC-STEM. Figure 4a shows that the engineered catalyst support 2Pt@CeO_2 contains atomically dispersed Pt species on the ceria support (circles in Fig. 4a), as also seen in both 1Pt@CeO_2 and 3Pt@CeO_2 reported in our previous study[24, 28]. After depositing Pd on the 2Pt@CeO_2 material, as shown in Fig. 4b, both single atoms and rafts with an average diameter of ca. 0.8 nm are present (Fig. 4b and Supplementary Figure 7). We note that the single atoms seen in these images come from Pt and not Pd, because the contrast of single atom Pd on ceria is not sufficient to make them visible in AC-STEM images (atomic number of Pd is lower than that of Ce, 46 vs 58). This is why we can only detect the clusters of Pd, and since the oxidation state cannot be inferred from this image, we will refer to them as Pd/PdO. The high magnification STEM-EDS mapping (Fig. 4c-f) shows that both Pt and Pd are well dispersed on this catalyst and the homogeneous contrast in a domain indicates that the Pd/PdO domains are not 3D clusters, which would generally show a brighter center. A

schematic view of the morphology of the Pd/PdO on 2Pt@CeO_2 is shown in the inset of Fig. 4b. The similarity in the image contrast of these Pd/PdO domains to the Pt clusters shown in Fig. 1 allows us to assign these as Pd/PdO 2-D rafts which are present on the atomically dispersed 2Pt@CeO_2.

The environment of the Pt and Pd atoms in the Pd/PdO 2-D rafts of the 1Pd/2Pt@CeO_2 catalyst was further examined via XAS measurements performed on the calcined samples (Fig. 5). The XANES spectrum of Pt edge of 1Pd/2Pt@CeO_2 shows that the Pt is oxidized (Fig. 5a), which is similar to the 1Pt@CeO_2 catalyst reported previously[27]. Likewise, the XANES spectrum of the Pd K edge of the as-prepared 1Pd/2Pt@CeO_2 resembles the bulk references PdO and $Pd(OAc)_2$. The EXAFS fits for these samples are shown in the supplementary materials (Supplementary Tables 3 - 8 and Supplementary Figures 8 - 13). The Pt L_3 edge EXAFS has one major peak due to Pt-O scattering, fitting gave a coordination number of 6±0.4 at a bond distance of 1.99±0.008 Å. A Pt-O coordination number of 6 is consistent with platinum in the +4 oxidation state. Previous reports on atom trapped Pt on CeO_2 gave a Pt-O coordination number of 5, the extra oxygen coordination likely comes from oxygen in the Pd/PdO rafts as seen in the STEM results[28]. The interface between the raft structure and the support is not strongly ordered as evidenced by a weak broad doublet peak at 2.8-3.4 Å (phase uncorrected distance) in the Pt EXAFS. The EXAFS at the Pd K edge for 1Pd/2Pt@CeO_2 resembles that of bulk PdO with attenuated 2nd and 3rd shell Pd-Pd scattering. Two models were used to fit the spectrum: a spherical PdO nanoparticle model, and a multi-shell PdO model without the shape function constraint. While both models gave equivalent reduced chi squared statistics, the R-factor for the multi-shell model was lower. This would be expected if the nanoparticle shape deviated from spherical. The misfit primarialy comes from underfitting the 2nd Pd-Pd coordination number. In a disk shaped particle, a spherical shape function will correctly model the data at distances lower than the shorter of the two characteristic lengths (radius and thickness) [43]. From the STEM results showing that the rafts are 1-2 atoms thick and based on the lattice parameter of PdO, the spherical model would start to fail past the first Pd-Pd path at 3.02 Å, which is seen in the misfit of the second Pd-Pd path in the spherical model. Consistent with the Pt L3 edge EXAFS, no Pd-Ce scattering was observed, which suggests a configurationally diverse interface between the raft and support.

We used surface-sensitive XPS to reveal differences in the Pd/PdO domains on the 1Pd/2Pt@CeO_2 compared to a reference (1Pd+2Pt)/CeO_2 sample prepared by conventional impregnation (Fig. 6). The reference sample (1Pd+2Pt)/CeO_2 sample shows significantly lower reactivity than the atom trapped 1Pd/2Pt@CeO_2 catalyst (Fig. 3a). The Pd 3d binding energy of Pd species on 1Pd/2Pt@CeO_2 is lower than that of the reference (1Pd+2Pt)/CeO_2 (Fig. 6b). This is suggestive of a different form of Pd oxide on the 1Pd/2Pt@CeO_2 surface, likely because it is present in the form of a raft, and different from 3D particles of bulk PdO present in the reference sample. The Pt 4f spectrum of 1Pd/2Pt@CeO_2 shows peaks at a higher binding energy in comparison to that of the reference (1Pd+2Pt)/CeO_2 (Fig. 6a), confirming

that the Pt species strongly bound to ceria via atom trapping in 1Pd/2Pt@CeO_2 are different from Pt that is deposited by impregnation and calcined at 500 ˚C in air. The trapping of the Pt is also confirmed by CO-DRIFTS experiments wherein the 1Pd/2Pt@CeO_2 catalyst shows the intense CO band on ionic Pt seen in previous work[24] (Supplementary Figure 14). The Pd in the 2-D rafts is mobile and transforms readily from its oxidized state into a reduced state during CO oxidation at 125 °C (Supplementary Figure 14). This mobility of Pd is consistent with previous studies of Pd single atom catalysts during CO oxidation[44, 45]. What is unique to the Pd/PdO structures stabilized by the single atom Pt is the enhanced reactivity for methane oxidation and improved water tolerance.

Based on the above characterization results and the negligible reactivity of the atom-trapped 2Pt@CeO_2 support in methane oxidation, we propose that the reactivity of the Pd deposited on atom-trapped 2Pt@CeO_2 (1Pd/2Pt@CeO_2) is associated with the 2-D Pd/PdO rafts which were detected via AC-STEM and EXAFS (Figs. 4 and 5). These rafts exhibit enhanced reactivity compared to the conventional 2Pt/CeO_2 and 1Pd/CeO_2 catalysts prepared via impregnation. The enhanced reactivity of 2-D Pd/PdO rafts in methane oxidation is confirmed by DFT calculations (Figs. 7a, b). A lower activation barrier (0.48 eV) for the methane activation is seen on the 2-D Pd/PdO rafts in which a single layer Pd atoms bonded to O atoms of CeO_2 to form Pd oxide rafts, as compared to that (0.80 eV) on metal Pd (111) and that (0.70 eV) on PdO (101). On the other hand, the exceptional water-tolerance of 1Pd/2Pt@CeO_2 in steam methane oxidation (10%H_2O vapor) can be explained based on DFT calculation results on the dissociation barrier of water molecule on the catalyst (Figs. 7c, d). The calculation results show that water molecule is easily dissociated to chemisorbed H* and OH* species with a low barrier of 0.23 eV when it is on PdO (111). This suggests that the produced OH* species, which has a large binding energy of -3.14 eV, could poison the PdO surface sites on the 1Pd/CeO_2 catalyst prepared by impregnation, leading to low activity for methane oxidation. While on 2-D Pd/PdO rafts and Pd (111), the barriers for the O-H bond cleavage in water is as high as 0.81 and 1.08 eV, respectively. Therefore, when exposed to steam, the 2-D Pd/PdO raft sites (i.e. 1Pd/2Pt@CeO_2 catalyst) are resistant to H_2O poisoning, leading to higher reactivity in methane oxidation. The intermediate behaviors of the Pd/PdO raft between the metallic (Pd (111)) and oxide (PdO (101)) forms originate from the partial oxidation of Pd by their bonding with substrate oxygens, as shown in Fig. 7.

4. Conclusions

In this study, we used atom-trapped Pt single atoms to modify and engineer the catalyst support to influence the nature of the deposited metal oxide. In the case of Pt deposited on atom-trapped 1Pt@CeO_2 (2Pt/1Pt@CeO_2), we found that 2-D Pt rafts were formed, the support formed prominent ceria (111) surface facets and the preferred orientation caused a higher surface Pt signal in LEIS. The 2-D Pt rafts showed higher reactivity in CO oxidation because of a weaker interaction between the Pt and the engineered support. The catalyst with the strongest interaction, 3Pt@CeO_2 had the lowest reactivity for CO oxidation. Using a similar atom trapping approach, we prepared a 1Pd/2Pt@CeO_2 which showed

much better reactivity than the conventional 1Pd/CeO_2, 2Pt@CeO_2 and (1Pd+2Pt)/CeO_2 catalysts containing the same number of metal atoms when tested for methane oxidation. Analogous to the case of 2Pt/1Pt@CeO_2, aberration-corrected electron microscopy results showed that the 1Pd/2Pt@CeO_2 catalyst presented Pd/PdO 2-D rafts with average size of 0.8 nm as well as the presence of Pt single atoms. Further methane oxidation results under the addition of 4-10 v/v% steam show that the 1Pd/2Pt@CeO_2 catalyst has improved water-tolerance in methane oxidation than conventional 1Pd/CeO_2 and (1Pd+2Pt)/CeO_2 catalysts. The critical difference is the nature of Pd/PdO phase in the 2-D rafts, which is similar to a surface oxide on Pd metal surface. The monolayer Pd oxide is not stable, since the Pd transforms readily to PdO phase, which is easily poisoned by water vapor. The superior water tolerance of the 1Pd/2Pt@CeO_2 catalyst is due to the presence of a different form of Pd oxide in the form of 2-D rafts on the engineered support via atom trapping. The performance of this Pd/PdO phase is very different from that of bulk PdO. The experimental observations are rationalized with model DFT calculations which show differences in the interaction of water vapor with the rafts compared with bulk PdO. This work demonstrates that the approach of atom trapping can be used to engineer a catalyst support leading to improved catalytic performance of the deposited phase. We suggest this approach could be added to the tool kit of catalyst designers to develop improved catalysts since the nucleation and growth of the deposited phase can be modified by the trapped atoms in the support.

Declarations

Acknowledgements

The catalyst synthesis and characterization via TEM and DRIFTS was supported by DOE/BES Catalysis Science program, grant DE-FG02-05ER15712. Reactivity measurements and Pt atom trapping calculations were supported by U.S. DOE Office of Energy Efficiency and Renewable Energy (EERE) under the Advanced Manufacturing Office, award number DE-LC 000L059. The computational work was supported by the National Natural Science Foundation of China (21673040 and 21973013) and Air Force Office of Scientific Research (FA9550-18-1-0413). The characterization via XAS was supported by the National Science Foundation under Cooperative Agreement No. EEC-1647722. Use of the Advanced Photon Source was supported by the U.S. Department of Energy Office of Basic Energy Sciences under contract no. DE-AC02-06CH11357. MRCAT operations, beamline 10-BM and 10-ID, are supported by the Department of Energy and the MRCAT member institutions. H. Xiong acknowledges support from the National High-Level Young Talents program and National Natural Science Foundation of China (22072118). We thank Arda Genc at Thermo-Fisher for providing the AC-STEM images and EDS maps of the catalysts. Sandia National Laboratories is a multi-mission laboratory managed and operated by National Technology and Engineering Solutions of Sandia, LLC, a wholly owned subsidiary of Honeywell International, Inc., for the U.S. Department of Energy's National Nuclear Security Administration under contract DE-NA0003525. This paper describes objective technical results and analysis. Any subjective views or opinions that might be expressed in the document do not necessarily represent the views of the U.S. Department of Energy or the United States Government.

References

1. Munnik, P.; de Jongh, P. E.; de Jong, K. P., Recent Developments in the Synthesis of Supported Catalysts. *Chemical Reviews* **2015,** *115* (14), 6687-6718.
2. Wong, A.; Liu, Q.; Griffin, S.; Nicholls, A.; Regalbuto, J. R., Synthesis of ultrasmall, homogeneously alloyed, bimetallic nanoparticles on silica supports. *Science* **2017,** *358* (6369), 1427-1430.
3. Bradley, S. A.; Sinkler, W.; Blom, D. A.; Bigelow, W.; Voyles, P. M.; Allard, L. F., Behavior of Pt Atoms on Oxide Supports During Reduction Treatments at Elevated Temperatures, Characterized by Aberration Corrected Stem Imaging. *Catalysis Letters* **2012,** *142* (2), 176-182.
4. Kwak, J. H.; Hu, J.; Mei, D.; Yi, C.-W.; Kim, D. H.; Peden, C. H. F.; Allard, L. F.; Szanyi, J., Coordinatively Unsaturated Al^{3+} Centers as Binding Sites for Active Catalyst Phases of Platinum on γ-Al_2O_3. *Science* **2009,** *325* (5948), 1670-1673.
5. Ding, K. L.; Cullen, D. A.; Zhang, L. B.; Cao, Z.; Roy, A. D.; Ivanov, I. N.; Cao, D. M., A general synthesis approach for supported bimetallic nanoparticles via surface inorganometallic chemistry. *Science* **2018,** *362* (6414), 560-564.
6. Bo, Z.; Ahn, S.; Ardagh, M. A.; Schweitzer, N. M.; Canlas, C. P.; Farha, O. K.; Notestein, J. M., Synthesis and stabilization of small Pt nanoparticles on TiO_2 partially masked by SiO_2. *Applied Catalysis A: General* **2018,** *551*, 122-128.
7. Yao, S.; Zhang, X.; Zhou, W.; Gao, R.; Xu, W.; Ye, Y.; Lin, L.; Wen, X.; Liu, P.; Chen, B.; Crumlin, E.; Guo, J.; Zuo, Z.; Li, W.; Xie, J.; Lu, L.; Kiely, C. J.; Gu, L.; Shi, C.; Rodriguez, J. A.; Ma, D., Atomic-layered Au clusters on α-MoC as catalysts for the low-temperature water-gas shift reaction. *Science* **2017,** *357* (6349), 389-393.
8. Chen, A.; Yu, X.; Zhou, Y.; Miao, S.; Li, Y.; Kuld, S.; Sehested, J.; Liu, J.; Aoki, T.; Hong, S.; Camellone, M. F.; Fabris, S.; Ning, J.; Jin, C.; Yang, C.; Nefedov, A.; Wöll, C.; Wang, Y.; Shen, W., Structure of the catalytically active copper–ceria interfacial perimeter. *Nature Catalysis* **2019,** *2* (4), 334-341.
9. Lu, J.; Elam, J. W.; Stair, P. C., Synthesis and Stabilization of Supported Metal Catalysts by Atomic Layer Deposition. *Accounts of Chemical Research* **2013,** *46* (8), 1806-1815.
10. Petrov, A. W.; Ferri, D.; Krumeich, F.; Nachtegaal, M.; van Bokhoven, J. A.; Kröcher, O., Stable complete methane oxidation over palladium based zeolite catalysts. *Nature Communications* **2018,** *9* (1), 2545.
11. Descorme, C.; Gélin, P.; Lécuyer, C.; Primet, M., Palladium-exchanged MFI-type zeolites in the catalytic reduction of nitrogen monoxide by methane. Influence of the Si/Al ratio on the activity and the hydrothermal stability. *Applied Catalysis B: Environmental* **1997,** *13* (3), 185-195.
12. Huang, W.; Goodman, E. D.; Losch, P.; Cargnello, M., Deconvoluting Transient Water Effects on the Activity of Pd Methane Combustion Catalysts. *Industrial & Engineering Chemistry Research* **2018,** *57* (31), 10261-10268.

13. Zhang, F.; Hakanoglu, C.; Hinojosa, J. A.; Weaver, J. F., Inhibition of methane adsorption on PdO(101) by water and molecular oxygen. *Surface Science* **2013,** *617*, 249-255.
14. Xiong, H.; Wiebenga, M. H.; Carrillo, C.; Gaudet, J. R.; Pham, H. N.; Kunwar, D.; Oh, S. H.; Qi, G.; Kim, C. H.; Datye, A. K., Design considerations for low-temperature hydrocarbon oxidation reactions on Pd based catalysts. *Applied Catalysis B: Environmental* **2018,** *236*, 436-444.
15. Karinshak, K. A.; Lott, P.; Harold, M. P.; Deutschmann, O., In situ Activation of Bimetallic Pd–Pt Methane Oxidation Catalysts. *ChemCatChem* **2020,** *12* (14), 3712-3720.
16. Lott, P.; Dolcet, P.; Casapu, M.; Grunwaldt, J.-D.; Deutschmann, O., The Effect of Prereduction on the Performance of Pd/Al_2O_3 and Pd/CeO_2 Catalysts during Methane Oxidation. *Industrial & Engineering Chemistry Research* **2019,** *58* (28), 12561-12570.
17. Hellman, A.; Resta, A.; Martin, N. M.; Gustafson, J.; Trinchero, A.; Carlsson, P. A.; Balmes, O.; Felici, R.; van Rijn, R.; Frenken, J. W. M.; Andersen, J. N.; Lundgren, E.; Grönbeck, H., The Active Phase of Palladium during Methane Oxidation. *The Journal of Physical Chemistry Letters* **2012,** *3* (6), 678-682.
18. Martin, N. M.; Van den Bossche, M.; Hellman, A.; Grönbeck, H.; Hakanoglu, C.; Gustafson, J.; Blomberg, S.; Johansson, N.; Liu, Z.; Axnanda, S.; Weaver, J. F.; Lundgren, E., Intrinsic Ligand Effect Governing the Catalytic Activity of Pd Oxide Thin Films. *ACS Catalysis* **2014,** *4* (10), 3330-3334.
19. Duan, H.; You, R.; Xu, S.; Li, Z.; Qian, K.; Cao, T.; Huang, W.; Bao, X., Pentacoordinated Al3+-Stabilized Active Pd Structures on Al_2O_3-Coated Palladium Catalysts for Methane Combustion. *Angewandte Chemie International Edition* **2019,** *58* (35), 12043-12048.
20. Johns, T. R.; Gaudet, J. R.; Peterson, E. J.; Miller, J. T.; Stach, E. A.; Kim, C. H.; Balogh, M. P.; Datye, A. K., Microstructure of Bimetallic Pt-Pd Catalysts under Oxidizing Conditions. *ChemCatChem* **2013,** *5* (9), 2636-2645.
21. Graham, G. W.; Jen, H. W.; Ezekoye, O.; Kudla, R. J.; Chun, W.; Pan, X. Q.; McCabe, R. W., Effect of alloy composition on dispersion stability and catalytic activity for NO oxidation over alumina-supported Pt–Pd catalysts. *Catalysis Letters* **2007,** *116* (1), 1-8.
22. Yashnik, S. A.; Chesalov, Y. A.; Ishchenko, A. V.; Kaichev, V. V.; Ismagilov, Z. R., Effect of Pt addition on sulfur dioxide and water vapor tolerance of Pd-Mn-hexaaluminate catalysts for high-temperature oxidation of methane. *Applied Catalysis B: Environmental* **2017,** *204*, 89-106.
23. Datye, A.; Wang, Y., Atom trapping: a novel approach to generate thermally stable and regenerable single-atom catalysts. *National Science Review* **2018,** *5* (5), 630-632.
24. Jones, J.; Xiong, H. F.; Delariva, A. T.; Peterson, E. J.; Pham, H.; Challa, S. R.; Qi, G. S.; Oh, S.; Wiebenga, M. H.; Hernandez, X. I. P.; Wang, Y.; Datye, A. K., Thermally stable single-atom platinum-on-ceria catalysts via atom trapping. *Science* **2016,** *353* (6295), 150-154.
25. Wei, S.; Li, A.; Liu, J.-C.; Li, Z.; Chen, W.; Gong, Y.; Zhang, Q.; Cheong, W.-C.; Wang, Y.; Zheng, L.; Xiao, H.; Chen, C.; Wang, D.; Peng, Q.; Gu, L.; Han, X.; Li, J.; Li, Y., Direct observation of noble metal nanoparticles transforming to thermally stable single atoms. *Nature Nanotechnology* **2018,** *13* (9), 856-861.

26. Goodman, E. D.; Johnston-Peck, A. C.; Dietze, E. M.; Wrasman, C. J.; Hoffman, A. S.; Abild-Pedersen, F.; Bare, S. R.; Plessow, P. N.; Cargnello, M., Catalyst deactivation via decomposition into single atoms and the role of metal loading. *Nature Catalysis* **2019,** *2* (9), 748-755.
27. Nie, L.; Mei, D.; Xiong, H.; Peng, B.; Ren, Z.; Hernandez, X. I. P.; DeLaRiva, A.; Wang, M.; Engelhard, M. H.; Kovarik, L.; Datye, A. K.; Wang, Y., Activation of surface lattice oxygen in single-atom Pt/CeO_2 for low-temperature CO oxidation. *Science* **2017,** *358* (6369), 1419-1423.
28. Kunwar, D.; Zhou, S.; DeLaRiva, A.; Peterson, E. J.; Xiong, H.; Pereira-Hernández, X. I.; Purdy, S. C.; ter Veen, R.; Brongersma, H. H.; Miller, J. T.; Hashiguchi, H.; Kovarik, L.; Lin, S.; Guo, H.; Wang, Y.; Datye, A. K., Stabilizing High Metal Loadings of Thermally Stable Platinum Single Atoms on an Industrial Catalyst Support. *ACS Catalysis* **2019,** *9* (5), 3978-3990.
29. Ravel, B.; Newville, M., ATHENA, ARTEMIS, HEPHAESTUS: data analysis for X-ray absorption spectroscopy using IFEFFIT. *Journal of Synchrotron Radiation* **2005,** *12* (4), 537-541.
30. Calvin, S.; Miller, M. M.; Goswami, R.; Cheng, S.-F.; Mulvaney, S. P.; Whitman, L. J.; Harris, V. G., Determination of crystallite size in a magnetic nanocomposite using extended x-ray absorption fine structure. *Journal of Applied Physics* **2003,** *94* (1), 778-783.
31. Kresse, G.; Hafner, J., Ab initio molecular dynamics for liquid metals. *Physical Review B* **1993,** *47* (1), 558-561.
32. Kresse, G.; Furthmüller, J., Efficient iterative schemes for ab initio total-energy calculations using a plane-wave basis set. *Physical Review B* **1996,** *54* (16), 11169-11186.
33. Kresse, G.; Joubert, D., From ultrasoft pseudopotentials to the projector augmented-wave method. *Physical Review B* **1999,** *59* (3), 1758-1775.
34. Huang, M.; Fabris, S., CO Adsorption and Oxidation on Ceria Surfaces from DFT+U Calculations. *Journal of Physical Chemistry C* **2008,** *112* (23), 8643-8648.
35. Perdew, J. P.; Chevary, J. A.; Vosko, S. H.; Jackson, K. A.; Pederson, M. R.; Singh, D. J.; Fiolhais, C., Atoms, molecules, solids, and surfaces: Applications of the generalized gradient approximation for exchange and correlation. *Physical Review B* **1992,** *46* (11), 6671-6687.
36. Henkelman, G.; Uberuaga, B. P.; Jónsson, H., A climbing image nudged elastic band method for finding saddle points and minimum energy paths. *Journal of Chemical Physics* **2000,** *113* (22), 9901-9904.
37. Henkelman, G.; Jónsson, H., Improved tangent estimate in the nudged elastic band method for finding minimum energy paths and saddle points. *Journal of Chemical Physics* **2000,** *113* (22), 9978-9985.
38. Pereira-Hernández, X. I.; DeLaRiva, A.; Muravev, V.; Kunwar, D.; Xiong, H.; Sudduth, B.; Engelhard, M.; Kovarik, L.; Hensen, E. J. M.; Wang, Y.; Datye, A. K., Tuning Pt-CeO_2 interactions by high-temperature vapor-phase synthesis for improved reducibility of lattice oxygen. *Nature Communications* **2019,** *10* (1), 1358.
39. Wang, H.; Liu, J.-X.; Allard, L. F.; Lee, S.; Liu, J.; Li, H.; Wang, J.; Wang, J.; Oh, S. H.; Li, W.; Flytzani-Stephanopoulos, M.; Shen, M.; Goldsmith, B. R.; Yang, M., Surpassing the single-atom catalytic

activity limit through paired Pt-O-Pt ensemble built from isolated Pt1 atoms. *Nature Communications* **2019,** *10* (1), 3808.

40. Datye, A. K.; Votsmeier, M., Opportunities and challenges in the development of advanced materials for emission control catalysts. *Nature Materials* **2020,** DOI: https://doi.org/10.1038/s41563-020-00805-3.
41. Dvořák, F.; Farnesi Camellone, M.; Tovt, A.; Tran, N.-D.; Negreiros, F. R.; Vorokhta, M.; Skála, T.; Matolínová, I.; Mysliveček, J.; Matolín, V.; Fabris, S., Creating single-atom Pt-ceria catalysts by surface step decoration. *Nature Communications* **2016,** *7* (1), 10801.
42. Xiong, H.; Lester, K.; Ressler, T.; Schlögl, R.; Allard, L. F.; Datye, A. K., Metastable Pd ↔ PdO Structures During High Temperature Methane Oxidation. *Catalysis Letters* **2017,** *147* (5), 1095-1103.
43. Glatter, O., The interpretation of real-space information from small-angle scattering experiments. *Journal of Applied Crystallography* **1979,** *12* (2), 166-175.
44. Jiang, D.; Wan, G.; Garcia-Vargas, C. E.; Li, L. Z.; Pereira-Hernandez, X. I.; Wang, C. M.; Wang, Y., Elucidation of the Active Sites in Single-Atom Pd_1/CeO_2 Catalysts for Low-Temperature CO Oxidation. *ACS Catalysis* **2020,** *10* (19), 11356-11364.
45. Spezzati, G.; Su, Y. Q.; Hofmann, J. P.; Benavidez, A. D.; DeLaRiva, A. T.; McCabe, J.; Datye, A. K.; Hensen, E. J. M., Atomically Dispersed Pd-O Species on CeO_2(111) as Highly Active Sites for Low-Temperature CO Oxidation. *ACS Catalysis* **2017,** *7* (10), 6887-6891.

Scheme

Scheme 1 is available as a Supplementary File.

Figures

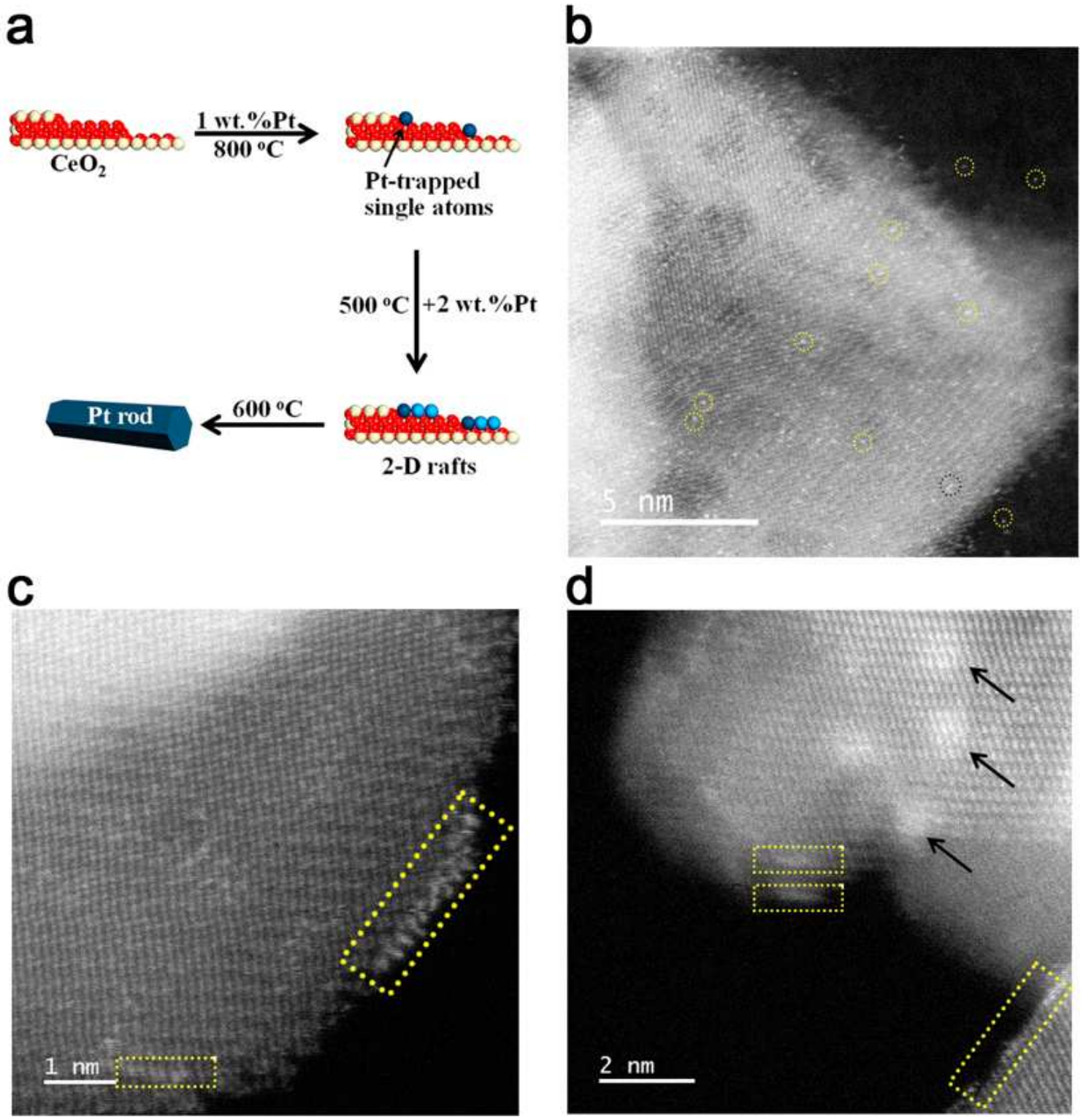

Figure 1

Transmission electron microscope images of 2-D rafts of Pt on Pt@CeO2. a, Schematic illustration showing the morphologies of Pt catalysts supported on ceria prepared by depositing Pt on a Pt-trapped ceria. The Pt atoms were labelled with different colors for the purpose of emphasizing the two steps in preparation. b, AC-STEM image of 1 wt.%Pt@CeO2 prepared by atom trapping showing atomically dispersed Pt indicated by circles. c,d, AC-STEM images of the catalyst prepared by depositing 2 wt% Pt on

atom trapped 1wt% Pt@CeO2. Edge-on views (c,d) indicated by rectangles show that Pt forms 2-D rafts which are approximately 1.5 nm in diameter as seen in top-down views indicated by arrows in (d). The uniform contrast of the particles in (d) confirms that these are not three-dimensional nanoparticles, which is a result of the modification of the catalyst support via atom trapping.

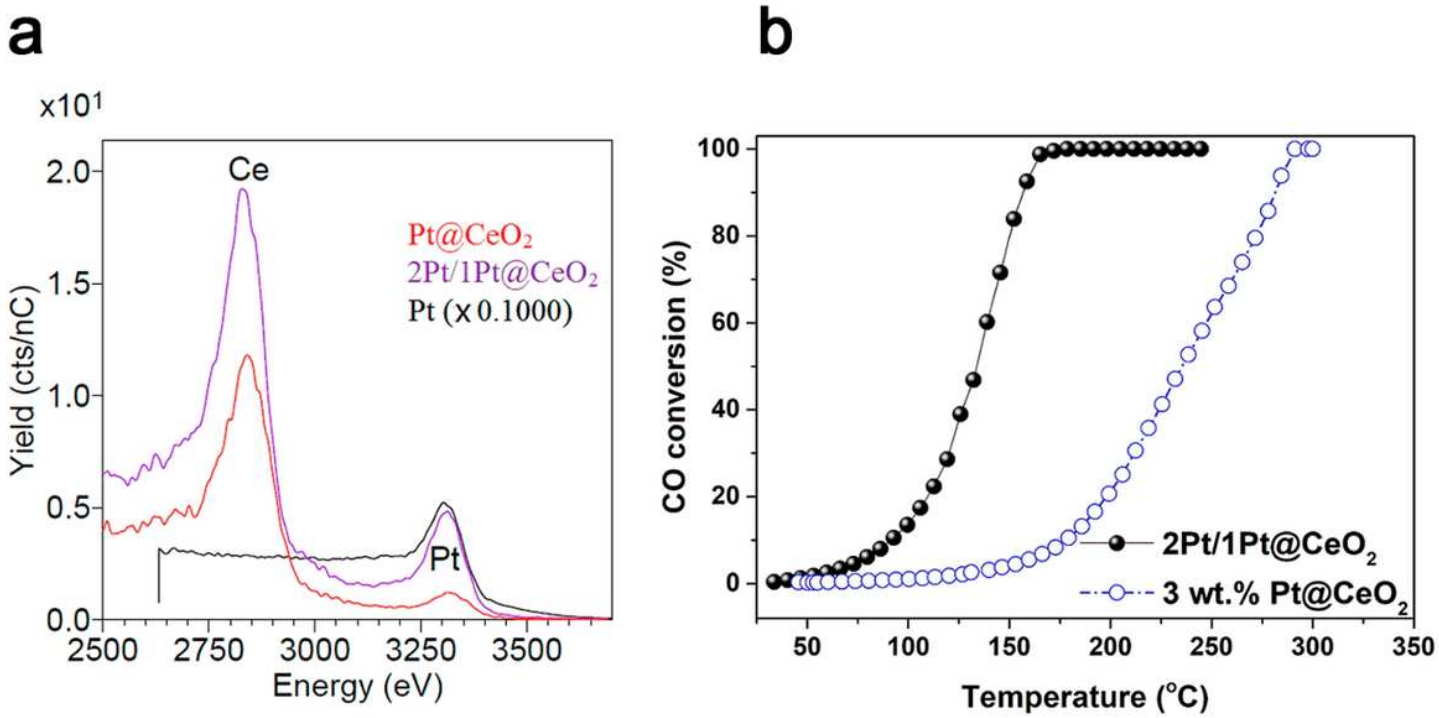

Figure 2

Low Energy Ion Scattering (LEIS) and CO oxidation reactivity of Pt 2D raft deposited on the engineered catalyst support. a, LEIS spectra of atomically dispersed 1Pt@CeO2 and 2Pt/1Pt@CeO2, the latter sample contains 2-D rafts of Pt as shown in Fig. 1. b, The CO oxidation reactivity confirms that the altered morphology of the Pt leads to enhanced CO oxidation reactivity. The 2-D Pt rafts (2Pt/1Pt@CeO2) are more active than the atom trapped catalyst 3Pt@CeO2. These two catalysts contain the same amount of Pt, the differences in reactivity can be attributed to different interaction with the support.

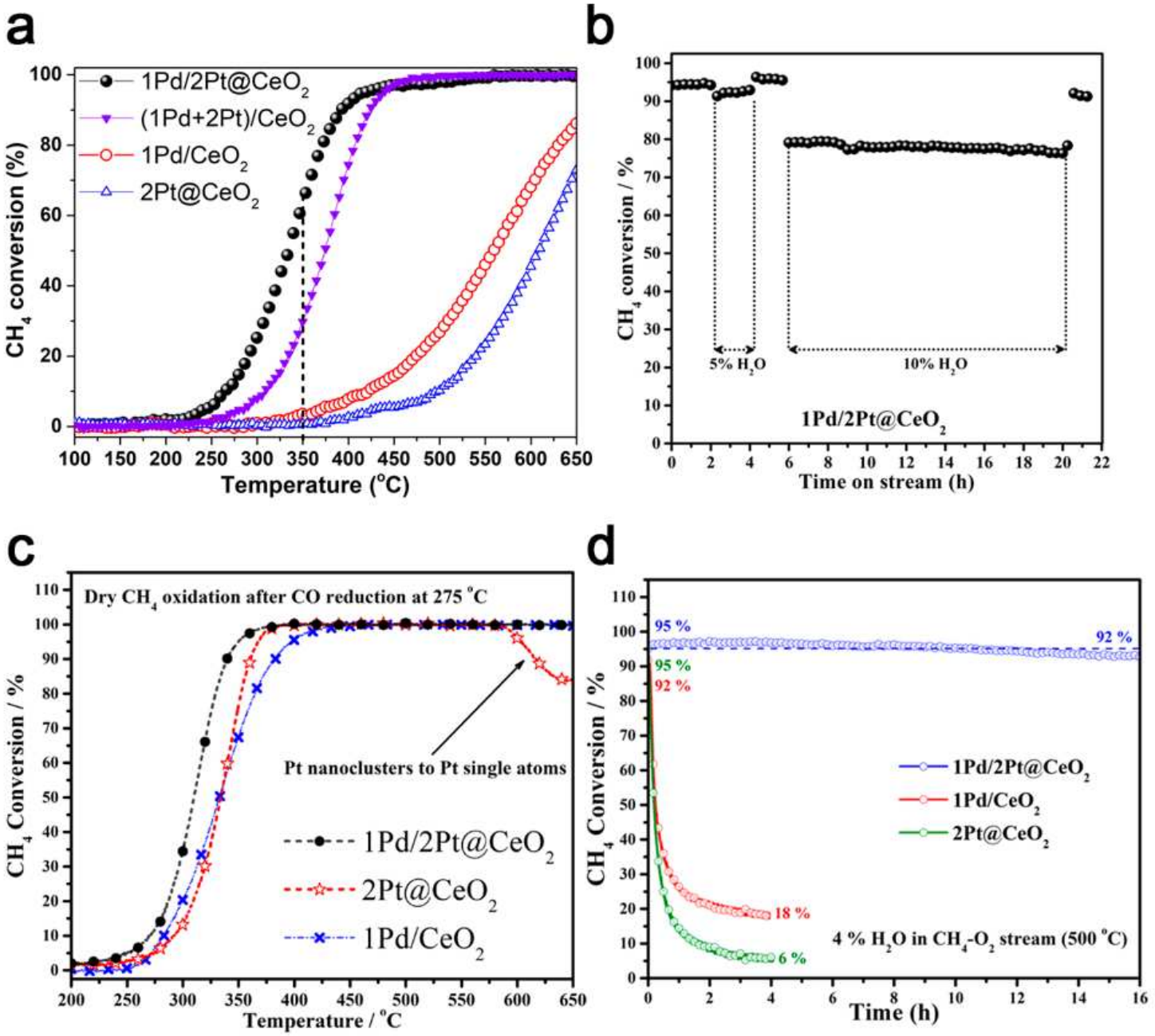

Figure 3

Methane oxidation reactivity of Pd-based catalysts with and without added water vapor. a, Light-off curves of CH4 oxidation under dry conditions over 1Pd/2Pt@CeO2, (2Pt+Pd)/CeO2 and 2Pt@CeO2 and 1Pd/CeO2 catalysts. b, Time-on-stream measurements for CH4 oxidation at 500 oC under different steam concentrations over 1Pd/2@CeO2 catalyst. c, Light-off curves of CH4 oxidation under dry conditions over reduced 1Pd/2Pt@CeO2 and 2Pt@CeO2 and Pd/CeO2 catalysts. d, Comparison of catalyst stability for 1Pd/2Pt@CeO2, reduced 2Pt@CeO2 and reduced 1Pd/CeO2 catalysts in CH4 oxidation at 500 oC in 4 % H2O showing the excellent water-tolerance of 1Pd/2Pt@CeO2.

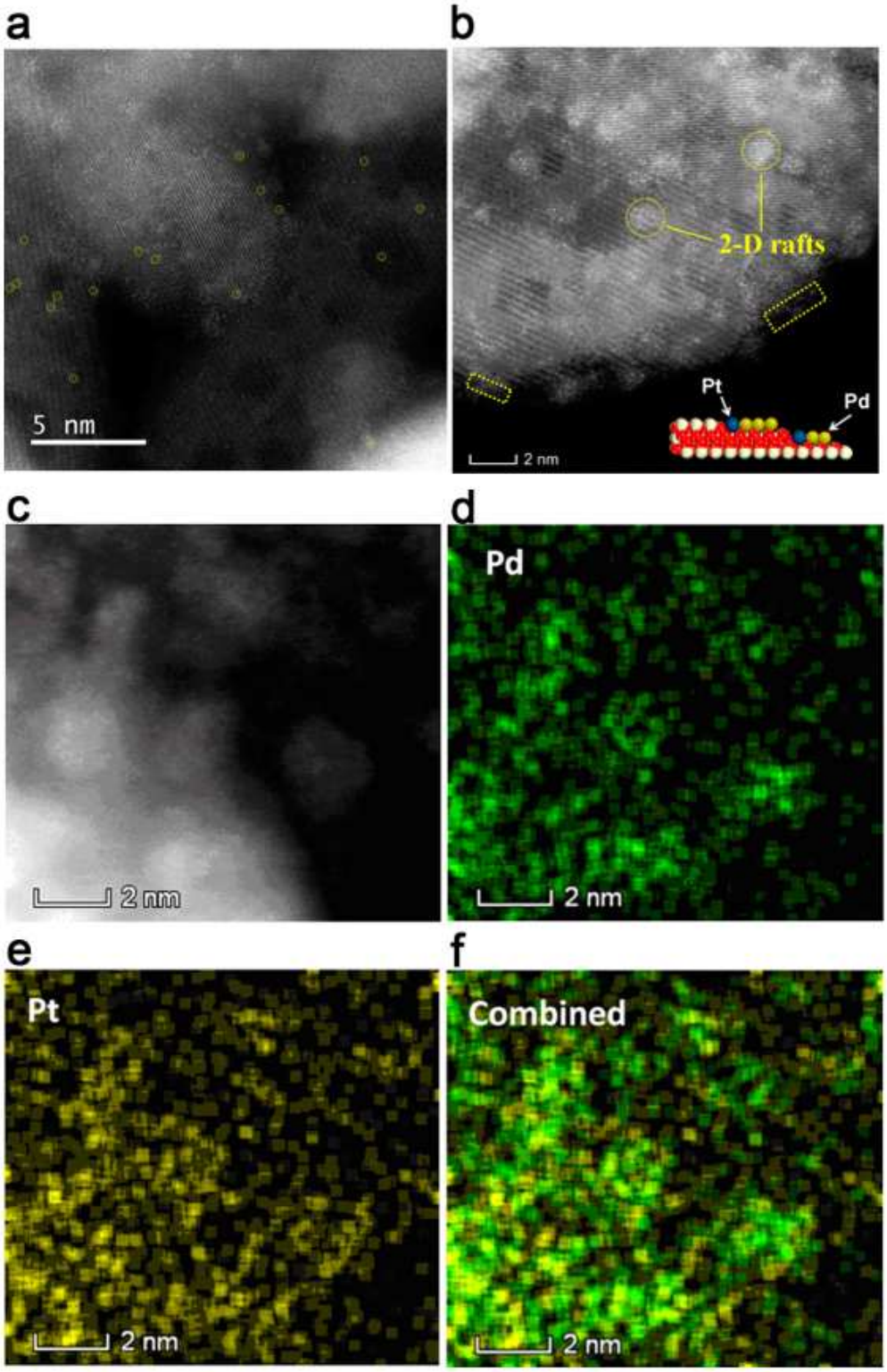

Figure 4

AC-STEM images of atom trapped 2Pt@CeO2 and 1Pd deposited on atom trapped 2Pt@CeO2 (1Pd/2Pt@CeO2). a, AC-STEM image of 2Pt@CeO2 prepared via atom trapping showing single atoms of Pt. b,c, AC-STEM image of Pd deposited on the catalyst shown in (a). 2-D rafts are visible which look similar to the 2-D rafts shown in Fig. 1c. d,e,f, STEM-EDS maps of this catalyst showing the Pd (d) and Pt (e) and the combined map indicating uniform distribution of Pd and Pt in the rafts.

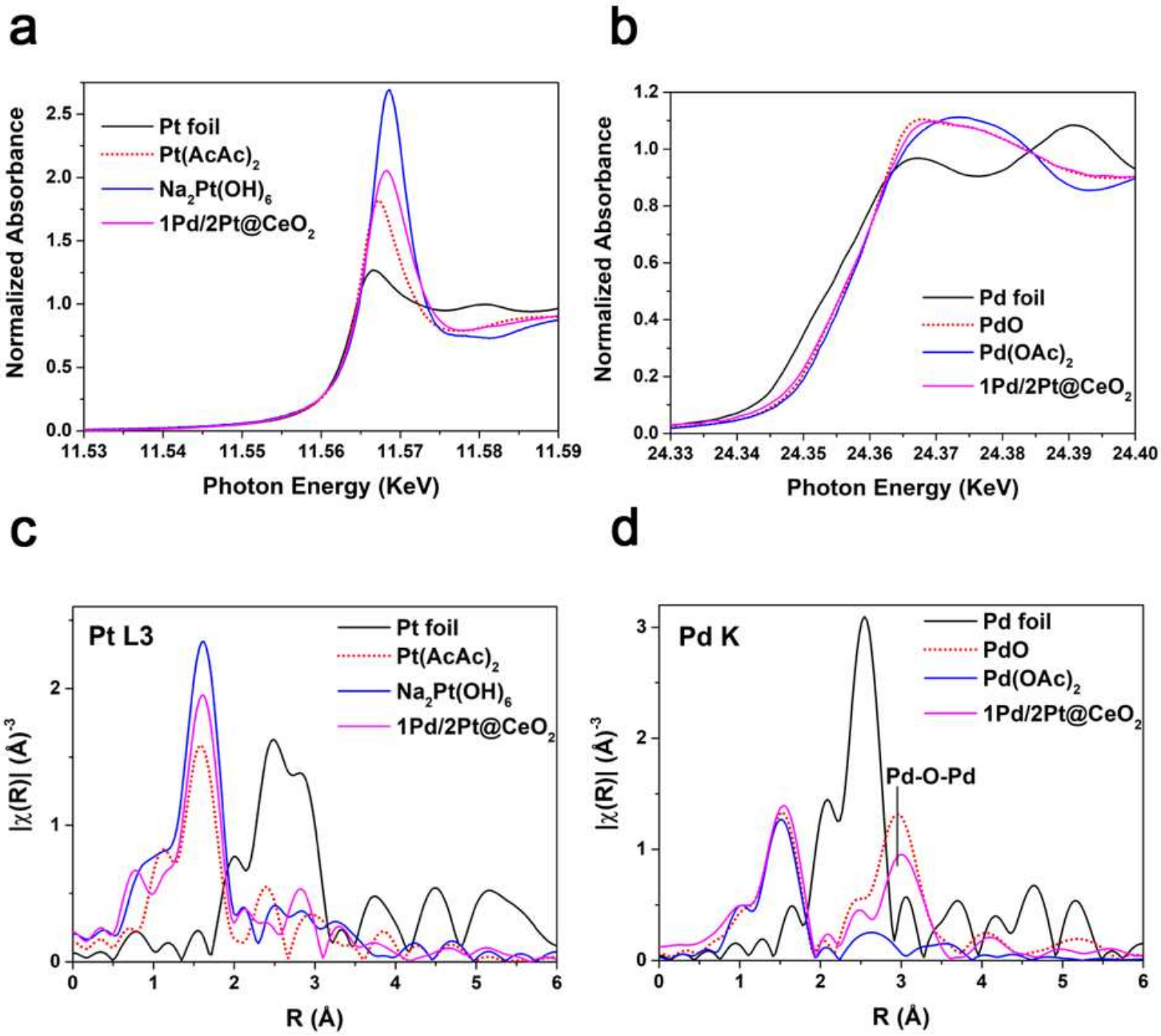

Figure 5

XAS spectra of 1Pd/2Pt@CeO2 sample. a,b, XANES spectra of Pt and Pd edges. c,d, EXAFS spectra of the Pt L and Pd K edges. The Pt and Pd standard samples were also measured.

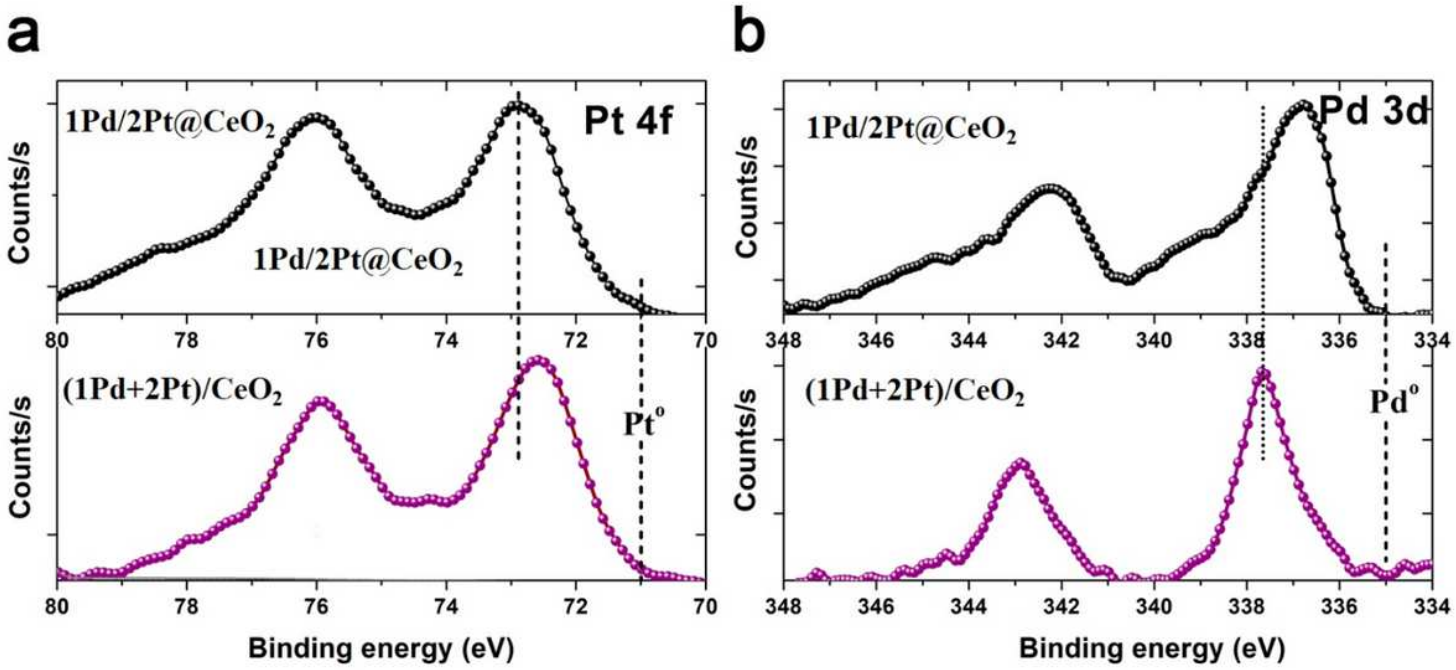

Figure 6

XPS spectra of 1Pd/2Pt@CeO2 and (1Pd+2Pt)/CeO2 catalysts. a, Pt 4f XPS spectra showing that the Pt in the catalyst prepared by atom trapping (1Pd/2Pt@CeO2) is different from Pt deposited by impregnation and calcination (1Pd+2Pt/CeO2). b, Pd 3d XPS spectra showing a clear difference between the sample prepared by deposition Pd on the atom-trapped Pt (1Pd/2Pt@CeO2) and the sample prepared by impregnation and calcination of the Pt and Pd precursors (1Pd+2Pt)/CeO2.

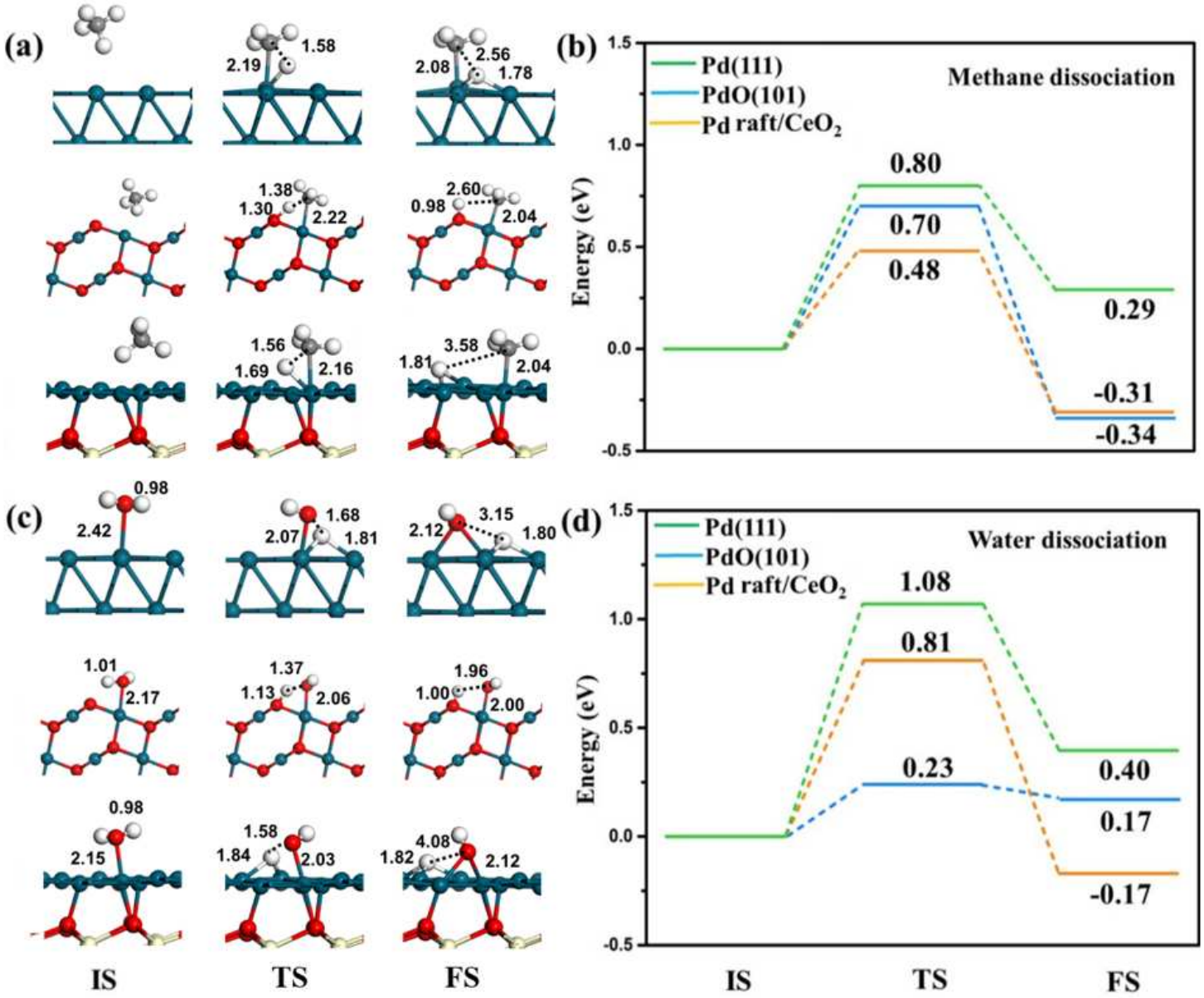

Figure 7

DFT simulations of (a-b) methane oxidation and (c-d) water dissociation over Pd, PdOand 2-D Pd rafts. a,b, Structures (the initial state (IS), transition state (TS) and final state (FS)) and the energy barriers of methane dissociation over the metal Pd(111), PdO(101) and CeO2(111) supported 2-D PdO raft. c,d, Structures (IS, TS and FS) and the energy barriers of water dissociation over the metal Pd(111), PdO(101) and CeO2(111) supported 2-D PdO raft. Color scheme: Ce, yellow; Pd, blue; O, red; C, grey; H, white.

Supplementary Files

This is a list of supplementary files associated with this preprint. Click to download.

- SupportinginformationforPtPdmanuscriptv4.pdf

- Scheme1.png